

---

# Impact of Patient Weight and Emission Scan Duration on PET/CT Image Quality and Lesion Detectability

Benjamin S. Halpern, MD<sup>1</sup>; Magnus Dahlbom, PhD<sup>1</sup>; Andrew Quon, MD<sup>1</sup>; Christian Schiepers, MD, PhD<sup>1</sup>; Christian Waldherr, MD<sup>1</sup>; Daniel H. Silverman, MD, PhD<sup>1</sup>; Osman Ratib, MD, PhD<sup>2</sup>; and Johannes Czernin, MD<sup>1</sup>

<sup>1</sup>Department of Molecular and Medical Pharmacology, Ahmanson Biological Imaging Center, David Geffen School of Medicine at UCLA, Los Angeles, California; and <sup>2</sup>Department of Radiological Sciences, David Geffen School of Medicine at UCLA, Los Angeles, California

---

This study was performed to prospectively evaluate fast PET/CT imaging protocols using lutetium oxyorthosilicate (LSO) detector technology and 3-dimensional (3D) image-acquisition protocols.

**Methods:** Fifty-seven consecutive patients (30 male, 27 female; mean age,  $58.6 \pm 15.7$  y) were enrolled in the study. After intravenous injection of 7.77 MBq (0.21 mCi) of <sup>18</sup>F-FDG per kilogram, a standard whole-body CT study (80–110 s) and PET emission scan were acquired for 4 min/bed position in 49 patients and 3 min/bed position in 8 patients. One-minute-per-bed-position data were then extracted from the 3- or 4-min/bed position scans to reconstruct single-minute/bed position scans for each patient. Patients were subgrouped according to weight as follows: <59 kg (<130 lb;  $n = 15$ ), 59–81 kg (130–179 lb;  $n = 33$ ), and  $\geq 82$  kg ( $\geq 180$  lb;  $n = 9$ ). Three experienced observers recorded numbers and locations of lesion by consensus and independently rated image quality as good, moderate, poor, or nondiagnostic. **Results:** The observers analyzed 220 reconstructed whole-body PET images from 57 patients. They identified 114 lesions ranging in size from 0.7 to 7.0 cm on the 3- ( $n = 8$ ) and 4-min/bed position images ( $n = 49$ ). Of these, only 4 were missed on the 1-min/bed position scans, and all lesions were identified on the corresponding 2-min/bed position images. One- and 2-min/bed position image quality differed significantly from the 4-min/bed position image reference ( $P < 0.05$ ). **Conclusion:** LSO PET detector technology permits fast 3D imaging protocols whereby weight-based emission scan durations ranging from 1 to 3 min/bed position provide similar lesion detectability when compared with 4-min/bed position images.

**Key Words:** lutetium oxyorthosilicate; PET/CT; molecular imaging

**J Nucl Med 2004; 45:797–801**

---

**T**he introduction of PET more than 2 decades ago has revolutionized oncologic imaging and fostered a new understanding of molecular alterations of cancer cells (1).

---

Received Jul. 29, 2003; revision accepted Jan. 12, 2004.  
For correspondence or reprints contact: Johannes Czernin, MD, Nuclear Medicine, UCLA School of Medicine, AR 128 CHS, 10833 Le Conte Ave., Los Angeles, CA 90095-6942.  
E-mail: jczernin@mednet.ucla.edu

<sup>18</sup>F-FDG PET imaging of tumor cell glycolysis has emerged as the most accurate tool for diagnosing, staging, restaging, and treatment monitoring of many malignancies (2,3).

However, anatomic information remains necessary to plan surgical interventions or radiation treatment. This cannot be provided by PET alone, a limitation that can be overcome by PET/CT imaging. Molecular and anatomic alterations can be imaged within a single examination, and nearly ideal fusion of molecular and anatomic images can be accomplished (4). This might result in improvements in diagnostic accuracy compared with PET alone (5–7).

Combined PET/CT imaging reduces the duration of PET imaging procedures, because the whole-body CT data can be used for photon attenuation correction. For conventional PET, attenuation correction is performed for each bed position using a traditional transmission source. This results in overall scan times of 50–70 min. Regardless of the PET detector crystals used, PET/CT imaging can reduce whole-body scanning times to 35 min or less.

Additional reductions in imaging times might be achieved with the utilization of lutetium oxyorthosilicate (LSO) detector technology. LSO has a higher light output and a shorter scintillation decay time than conventional bismuth germanate (BGO) detectors, resulting in markedly improved counting-rate capabilities (8,9). These features permit whole-body PET images to be acquired in the 3-dimensional (3D) mode, thereby greatly enhancing the sensitivity of the PET scanner.

The purpose of the current study was to evaluate prospectively whether the LSO detector technology together with 3D data acquisition can result in further shortening of imaging protocols without compromising lesion detectability in whole-body PET/CT imaging.

## MATERIALS AND METHODS

### Patients

The study population included 57 consecutive patients (mean age,  $58.6 \pm 15.7$  y) who underwent clinical PET/CT studies for staging or restaging of lung cancer ( $n = 15$ ), lymphoma ( $n = 12$ ),

breast cancer ( $n = 9$ ), colorectal cancer ( $n = 9$ ), unknown primary ( $n = 5$ ), sarcoma ( $n = 2$ ), ovarian cancer ( $n = 1$ ), squamous cell carcinoma of the neck ( $n = 1$ ), thyroid cancer ( $n = 1$ ), melanoma ( $n = 1$ ), and Erdheim-Chester disease ( $n = 1$ ).

Patient weight averaged  $70 \pm 13$  kg ( $153 \pm 28$  lb), ranging from 41 to 102 kg (90–225 lb). To determine the effect of patient weight on lesion detectability and image quality, the study population was subclassified as follows: group 1,  $<59$  kg ( $<130$  lb;  $n = 15$ ); group 2, 59–81 kg (130–179 lb;  $n = 33$ ); and group 3,  $\geq 82$  kg ( $\geq 180$  lb;  $n = 9$ ).

To determine the incidence of overweight and obesity in the study population, body mass index was calculated for each patient. Body mass indices of  $<20$ , 20–25,  $>25$ – $<30$ , and  $\geq 30$  were categorized as underweight, normal weight, overweight, and obese, respectively (10).

### Image Acquisition

Images were obtained using the Reveal RT PET/CT scanner (CPS Innovations). The PET part of the system, which is an ECAT ACCEL, acquires 47 transaxial images simultaneously and consists of 3 rings with a total of 144 LSO block detectors. Each block contains 64 crystals ( $6.75 \times 6.75 \times 20$  mm deep), covering an axial field of view (FOV) of 15 cm and a transaxial FOV that is 60 cm in diameter. The transaxial spatial resolution varies from 6.0 mm in full width at half maximum (FWHM) at the center of the FOV and a 6.7-mm FWHM radially at a radius of 10 cm. The average axial resolution changes from 4.5 mm at the center to a 5.9-mm FWHM at a radius of 10 cm. The interplane spacing is 3.4 mm. Because the system does not have interplane septa, PET images are acquired in 3D mode. This is a high-sensitivity acquisition mode whereby coincidence events are detected from the entire volume within the scanner FOV rather than from a set of adjacent thin slices, as is the case for 2-dimensional (2D) data acquisition.

The CT component of the PET/CT system is a conventional Somatom Duo (Siemens), a dual-slice helical CT scanner. This system is capable of acquiring an entire torso scan (100 cm) in less than 80 s. The CT scanner is also capable of acquiring all standard clinical CT protocols. Together with the PET system, the CT scanner is used both for attenuation correction of the PET data and for localization of  $^{18}\text{F}$ -FDG uptake in the PET images.

All patients fasted for at least 6 h before PET/CT. Sixty minutes after intravenous injection of 7.77 MBq (0.21 mCi) of  $^{18}\text{F}$ -FDG per kilogram, all patients were positioned on the imaging table in the arms-up position.

After determining the imaging field with an initial scout scan, an 80- to 110-s whole-body CT acquisition was performed using the following parameters: 130 kVp, 120 mA, 1-s tube rotation, 4-mm slice collimation, and a bed speed of 8 mm/second (i.e., pitch = 1). Upon completion of the CT portion, PET emission data were acquired for 3 min/bed position ( $n = 8$ ) or 4 min/bed position ( $n = 49$ ). Six to 8 bed positions were imaged per patient, resulting in whole-body PET emission scan durations ranging from 18 to 32 min. Patients were instructed to use shallow breathing, because this has been shown to minimize misregistrations and attenuation artifacts between PET and CT images (11).

### Image Reconstruction

The CT images were reconstructed using the algorithm developed at the University of Pittsburgh. In this approach, Hounsfield units in the CT images are scaled to appropriate attenuation coefficients at 511 keV (4,12).

CT images were used for attenuation correction and lesion localization. PET images were reconstructed using iterative algorithms (ordered-subset expectation maximization [OSEM], 2 iterations, 8 subsets) to a final image resolution of 8.8 mm FWHM.

Single-minute frames were extracted from the 3- or 4-min/bed position images using the raw sinogram datasets. To generate these single-minute frames, the recorded true and accidental coincidence events at each bed position were randomly subsampled. For example, to generate a 1-min frame, one quarter of all coincidence events were sampled from the 4-min/bed position data without replacement. The subsampled datasets were subsequently reconstructed and assembled into whole-body image sets.

### Image Analysis

First, the completed 220 image sets (8 patients with 3-min/bed position images and 49 patients with 4-min/bed position images) were presented to 3 experienced nuclear medicine physicians in a random sequence as follows:

Lesions were identified by consensus and were recorded for each whole-body image set.  $^{18}\text{F}$ -FDG uptake was considered abnormal if it was focal and greater than background activity.

For quality assessment, images were windowed at each interpreter's preference. Each experienced reader then graded image quality subjectively as good, moderate, poor, or nondiagnostic. In general, smoothness versus graininess of the liver was used as a criterion to distinguish poor from moderate quality. Image sharpness, usually seen best in the thorax at the junction of the lung and chest wall, was used to distinguish good from moderate quality.

Regions of interest (ROI) were placed around the lesions, and maximum and mean standardized uptake values (SUVs) were obtained for all recorded lesions (13).

Finally, to determine lesion size, bidimensional diameters of all lesions were derived from axial CT images using calipers.

### Statistical Analysis

For the quality assessment, agreement between readers was evaluated using  $\kappa$ -statistics.  $\kappa$ -values  $> 0.80$  indicated almost perfect concordance, and  $\kappa$ -values of 0.61–0.80 indicated substantial agreement (14).

The relationship between acquisition time and image quality was evaluated with a generalized estimating equations (GEE) model. A logit-link function and multinomial distribution with marginal model were used, and the  $\chi^2$  value was determined (15).

## RESULTS

### Lesion Distribution, Lesion Size, and SUV

A total of 114 hypermetabolic lesions were identified. Of these, 72 (63%) were localized in the chest, 16 (14%) in the abdomen, 14 (12%) in the head and neck region, and 12 (12%) in the pelvis. Chest lesions were most prevalent in all 3 weight groups, followed by abdominal lesions, head and neck lesions, and pelvic lesions.

Lesions ranged in size from 0.7 to 7.0 cm. Table 1 details lesion size stratified by weight groups. Sixty-five percent of the lesions were smaller than 2 cm and 16% were smaller than 1 cm.

Mean and maximum SUVs ranged from 0.3 to 9.8 and 0.7 to 16.7, respectively. All hypermetabolic lesions corresponded to anatomic abnormalities on CT.

**TABLE 1**  
Lesion Size and Maximum SUV for Weight Groups

Characteristic	Weight groups ( <i>n</i> = 114)		
	<59 kg (%)	59–81 kg (%)	≥82 kg (%)
Lesion size			
<1 cm	6 (21)	8 (11)	4 (37)
1–2 cm	14 (50)	40 (53)	2 (18)
2–3 cm	5 (18)	16 (21)	2 (18)
≥3 cm	3 (11)	11 (15)	3 (27)
SUV max			
<2.5	11 (39)	31 (41)	3 (27)
≥2.5	17 (61)	44 (59)	8 (73)

*n* = number of lesions; SUV max = maximum SUV.

Maximum SUVs stratified by weight groups are also listed in Table 1. Thirty-nine percent of lesions had maximum SUVs below 2.5.

Thus, the study sample included a considerable number of small, only mildly hypermetabolic lesions.

### Lesion Detectability

On the 3- and 4-min/bed position images, a total of 114 hypermetabolic lesions were identified. Of these, 110 (96.5%) were also detected on all 1- and 2-min/bed position images. Four small lesions (range, 0.9–1.3 cm) were missed on whole-body images assembled from 1-min/bed position scans. Three of these were located in the chest and one in the abdomen. Their mean and maximum SUV ranged from 0.3 to 2.6 and from 0.6 to 3.6 on 3- and 4-min/bed position images, respectively.

Twenty-eight lesions were identified in weight category 1, 75 in category 2, and 11 in category 3. When classified by body mass index, 17 lesions occurred in underweight patients, 40 in the normal weight group, 46 in overweight patients, and 11 in obese patients. The relationship between body mass index, SUV, and lesion size is presented in Table 2.

All lesions identified on the longest acquisition duration (3 or 4 min/bed position) in category 1 were also noted on all other images (i.e., on 1-, 2-, or 3-min/bed position images (Fig. 1).

In category 2, 2 lesions were missed on 1-min/bed position frames but were detected on all other images (Fig. 2). Similarly, 2 lesions were missed in category 3 on 1-min/bed position images but were detected on all other image frames.

Thus, 1-min/bed position emission scans were sufficient to detect all lesions in patients weighing less than 59 kg (130 lb). Two-minute/bed position emission scans were sufficient to detect all lesions in all weight groups when 4-min/bed position images were used as the reference standard.

### Image Quality

The interpreters' concordance on image quality was good, as determined by  $\kappa$ -statistics (Table 3). Comparison

of the image quality for the 3 different acquisition times with the reference standard of 4 min/bed position with the GEE model yielded the following  $\chi^2$  values:  $P < 0.05$  for 1 min/bed position,  $P < 0.05$  for 2 min/bed position, and  $P = 0.11$  for 3 min/bed position. Thus, statistical analysis revealed that the image quality of the 1- and 2-min/bed position scans was significantly different from that of the 4-min/bed position reference standard. However, 3-min/bed position image quality only tended to be better than the quality of 4-min/bed position scans.

### DISCUSSION

The current study demonstrated that LSO detector technology, together with a 3D image-acquisition mode, permitted emission scans of 1 min/bed position in patients who weighed less than 59 kg (130 lb), without compromising lesion detectability when 4-min/bed position images were used as a reference standard. However, because 4 lesions were missed on 1-min/bed position scans, such short scan durations should not be used in patients with higher weights. Two-minute/bed position emission scans were sufficient to detect all lesions identified on 4-min/bed position images in the study population. As expected, image quality varied significantly among different scan durations.

Using a BGO PET scanner and 2D data acquisition, Dahlbom et al. (16) were the first to demonstrate that non-attenuation-corrected scan times could be reduced to 1–2 min/bed position without compromising image quality. However, this study did not systematically analyze the effect of short PET acquisition protocols on lesion detectability.

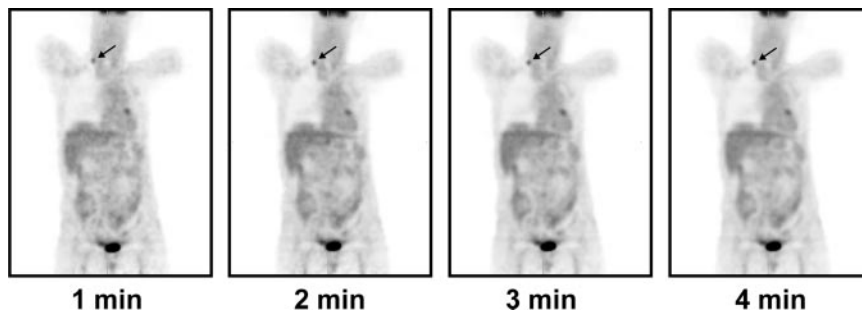
Conventional PET uses rotating  $^{68}\text{Ge}$  sources to obtain transmission scans that are used for photon attenuation correction. Frequently, these transmission images are acquired for 3–5 min/bed position, thereby adding considerable time to the image acquisition protocols (17). In contrast, attenuation correction for PET/CT is accomplished by using whole-body CT images, which are acquired in 80–

**TABLE 2**  
Lesion Size and Maximum SUV for Body Mass Index Groups

Characteristic	Body mass index ( <i>n</i> = 114)		
	Underweight, <20 (%)	Normal, 20–25 (%)	Overweight and obese, ≥25 (%)
Lesion size			
<1 cm	3 (17)	7 (18)	8 (14)
1–2 cm	10 (59)	16 (40)	30 (53)
2–3 cm	2 (12)	9 (22)	12 (21)
≥3 cm	2 (12)	8 (20)	7 (12)
SUV max			
<2.5	6 (35)	14 (35)	25 (44)
≥2.5	11 (65)	26 (65)	32 (56)

*n* = number of lesions; SUV max = maximum SUV.

**FIGURE 1.** Patient (77 y old; weight, 58 kg [128 lb]) with lung cancer, after radiation and surgical resection. Small focus of increased glycolytic activity was identified on whole-body images assembled from 1-, 2-, 3-, and 4-min/bed position images. This corresponded to a subcentimeter, right-sided supraclavicular lymph node on CT images.



110 s with the dual-detector CT used in the current study (12). Thus, all PET/CT devices, regardless of detector technology, allow for a shortening of overall imaging time. However, the high counting rate capability of LSO detectors permits a further reduction of imaging time.

The main goal of the current study was to determine whether fast, weight-based PET/CT imaging protocols could be established without compromising lesion detectability. To evaluate this approach, the raw sinogram datasets obtained in all patients were subsampled (in terms of acquisition time) to shorter acquisition frames from the original 3- or 4-min/bed position datasets.

As expected, image quality declined with reduced emission scan duration. This is because the number of measured counts was reduced by a factor of 4 when the image acquisition time was reduced from 4 to 1 min/bed position. However, this decrease in collected counts was offset, at least in part, by the high counting rate capability of the LSO detector material. Lesion detectability in comparison with the 4-min/bed position standard was not affected when a weight-based protocol was used.

Shorter image acquisition times increase image noise. The lack of false-positive findings in the current study, despite such increased noise levels, was therefore surprising. This was probably a result of the facts that all readers were experienced and that image noise, most prominently in the liver, can almost always be recognized as such. It is, however, conceivable that short image acquisition times resulting in noisy images might increase the number of false-positive findings in larger study populations.

Four lesions were not detected on 1-min/bed position images and were thus false-negative when using the reference standard of 4-min/bed position scans. However, le-

sions might have been missed on the 4-min/bed position scan, and the true number of false-negative scans is difficult to determine. It should be mentioned that after the analysis of all PET studies was completed, all whole-body CT images were inspected and reviewed for anatomic lesions that were not hypermetabolic on PET images. No such additional lesions were found.

This study had several limitations. These include the lack of a pathology gold standard, use of a 4-min/bed position image as the reference standard, risk of recognition bias, and inhomogeneous lesion distribution between and within different weight groups. Finally, the effects of varying scan durations on inter- and intraobserver variability were not assessed.

No attempt was made to verify whether focally increased <sup>18</sup>F-FDG uptake corresponded to malignant or benign lesions. Thus, with regard to underlying pathology, no gold standard was provided. The study, however, was not undertaken to determine diagnostic accuracy but rather to compare lesion detectability between different scan durations regardless of underlying pathology.

The image acquisition and reconstruction algorithm used might have affected the results of this study. The OSEM algorithm with 2 subsets and 8 iterations may have resulted in overly smooth images, thereby reducing detectability of small lesions even on 4-min/bed position scans. This would have biased the results in favor of good lesion detectability with 1-min/bed position images. However, we elected to use a standard imaging protocol as the reference standard (i.e., 4 min/bed position) and a standard reconstruction protocol as suggested by the vendor. This might not be the best way to reconstruct images, but it is the most frequently used clinical approach for this type of PET/CT system. On the

**FIGURE 2.** Patient (46 y old; weight 73 kg [160 lb]) with non-small cell lung cancer. Small focus of increased uptake corresponded to 1.3-cm primary lung cancer. On prospective evaluation, this lesion had been missed on 1-min/bed position images.

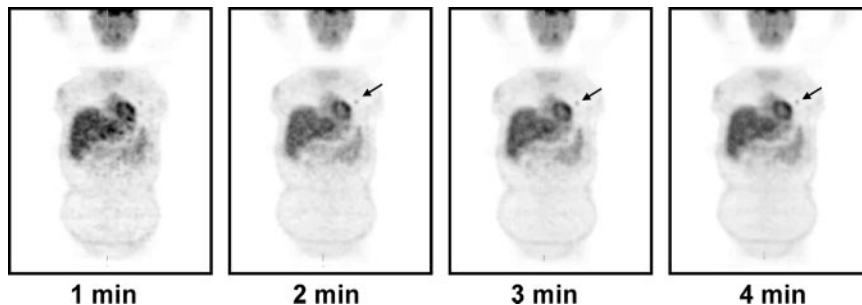


**TABLE 3**  
Image Quality and Reader Agreement\*

Quality	Reader 1	Reader 2	Reader 3
Nondiagnostic	0	0	1
Poor	30	25	32
Moderate	92	92	93
Good	98	103	94

\* $\kappa$ -values for agreement were 0.71 for reader 1 vs. reader 2, 0.76 for reader 1 vs. reader 3, and 0.69 for reader 2 vs. reader 3.

other hand, a bias in favor of longer acquisition times might have arisen from extracting short image frames, because this approach eliminates the effects of patient motion.

A recognition bias with regard to lesion identification cannot be ruled out in the current study. This was minimized by using a block design, whereby a random sequence of only a single complete set of coronal, axial, and sagittal images per patient was presented within a block to the readers. To further minimize the risk of recognition bias, the images were presented to the readers over a time period of more than 6 mo.

The results of the study might be affected by lesion localization. Sixty-three percent of all lesions occurred in the chest, a location that facilitates lesion detectability. However, this study was designed prospectively in a population with unpredictable lesion location. In addition, lung cancer, lymphoma, and breast cancer were the most frequent referral diagnoses for the clinical PET/CT study. These cancers are more frequently associated with metastatic disease to the chest than to the abdomen or pelvis.

Shorter scan times associated with higher image noise levels might result in increased inter- and intraobserver variability. However, no such analysis was performed in the current study. We attempted to reproduce the clinical read-out situation that, at our institution, always involves multiple readers. We thus opted for a consensus interpretation. Determination of intraobserver variability was not possible, because such analysis would have greatly increased the risk for recognition bias. Thus, these issues should be addressed in future studies.

## CONCLUSION

We have clinically implemented the weight-based PET imaging protocol described here for all patients and to date have studied more than 2,000 patients. In patients weighing less than 59 kg (130 lb), we are routinely obtaining whole-body PET/CT scans in 7 or 8 min, depending on the number of bed positions used. The maximum imaging time in patients weighing more than 114 kg (250 lb) is about 35 min.

Such rapid imaging protocols have advantages. First, virtually all patients can be studied in the arms-up position, avoiding beam-hardening artifacts from CT (18). Second, shorter imaging times are likely to reduce patient motion and thus improve image fusion. Third, a short imaging protocol permits more efficient use of expensive equipment. Fourth, shorter image acquisition protocols using PET/CT are convenient for patients. Finally, even the addition of CT contrast studies results in image acquisition times of less than 1 h. The implementation of this protocol has reduced PET whole-body imaging times to an average of less than 14 min per patient in our institution.

## ACKNOWLEDGMENT

We appreciate the help of James W. Sayre, PhD, with the statistical analysis.

## REFERENCES

1. Phelps ME, Hoffman EJ, Huang SC, Kuhl DE. ECAT: a new computerized tomographic imaging system for positron-emitting radiopharmaceuticals. *J Nucl Med.* 1978;19:635–647.
2. Gambhir SS, Czernin J, Schwimmer J, Silverman DH, Coleman RE, Phelps ME. A tabulated summary of the FDG PET literature. *J Nucl Med.* 2001;42:1S–93S.
3. Dwamena BA, Sonnad SS, Angobaldo JO, Wahl RL. Metastases from non-small cell lung cancer: mediastinal staging in the 1990s—meta-analytic comparison of PET and CT. *Radiology.* 1999;213:530–536.
4. Beyer T, Townsend DW, Brun T, et al. A combined PET/CT scanner for clinical oncology. *J Nucl Med.* 2000;41:1369–1379.
5. Lardinois D, Weder W, Hany TF, et al. Staging of non-small-cell lung cancer with integrated positron-emission tomography and computed tomography. *N Engl J Med.* 2003;348:2500–2507.
6. Hany TF, Steinert HC, Goerres GW, Buck A, von Schulthess GK. PET diagnostic accuracy: improvement with in-line PET-CT system: initial results. *Radiology.* 2002;225:575–581.
7. Antoch G, Stattaus J, Nemat AT, et al. Non-small cell lung cancer: dual-modality PET/CT in preoperative staging. *Radiology.* 2003;229:526–533.
8. Nutt R. For: Is LSO the future of PET? *Eur J Nucl Med Mol Imaging.* 2002;29:1523–1525.
9. Chatziioannou AF, Cherry SR, Shao Y, et al. Performance evaluation of micro-PET: a high-resolution lutetium oxyorthosilicate PET scanner for animal imaging. *J Nucl Med.* 1999;40:1164–1175.
10. National Institutes of Health. *Clinical Guidelines on the Identification, Evaluation and Treatment of Overweight and Obesity in Adults. The Evidence Report.* Bethesda, MD: National Institutes of Health; 1998. NIH publication 98-4083.
11. Goerres GW, Burger C, Kamel E, et al. Respiration-induced attenuation artifact at PET/CT: technical considerations. *Radiology.* 2003;226:906–910.
12. Kinahan PE, Townsend DW, Beyer T, Sashin D. Attenuation correction for a combined 3D PET/CT scanner. *Med Phys.* 1998;25:2046–2053.
13. Zasadny KR, Wahl RL. Standardized uptake values of normal tissues at PET with 2-[fluorine-18]-fluoro-2-deoxy-D-glucose: variations with body weight and a method for correction. *Radiology.* 1993;189:847–850.
14. Landis JR, Koch GG. The measurement of observer agreement for categorical data. *Biometrics.* 1977;33:159–174.
15. Zeger SL, Liang KY. Longitudinal data analysis for discrete and continuous outcomes. *Biometrics.* 1986;42:121–130.
16. Dahlbom M, Hoffman EJ, Hoh CK, et al. Whole-body positron emission tomography. Part I. Methods and performance characteristics. *J Nucl Med.* 1992;33:1191–1199.
17. Bailey DL. Transmission scanning in emission tomography. *Eur J Nucl Med.* 1998;25:774–787.
18. Zatz LM, Alvarez RE. An inaccuracy in computed tomography: the energy dependence of CT values. *Radiology.* 1977;124:91–97.